

**September 17, 2009**

## **DOE Final Report for DE-FG02-99ER45778**

### **Design and Fabrication of Photonic Crystals for Thermal Energy Conservation**

#### ***Progress during this final period:***

The focus of the research for our last year of funding was on the exploration of the possibility of incorporating, for the first time, crystalline materials rather than the ubiquitous glassy materials in a fiber material system. The reasons for this are the following.

The vision of intelligent and large-area fabrics capable of signal processing, sensing and energy harvesting has made incorporating electronic devices into flexible fibers an active area of research. Fiber-integrated rectifying junctions in the form of photovoltaic cells and light-emitting diodes (LEDs) have been fabricated on optical fiber substrates. However, the length of these fiber devices has been limited by the processing methods and the lack of a sufficiently conductive and transparent electrode. Their cylindrical device geometry is ideal for single device architectures, like photovoltaics and LEDs, but not amenable to building multiple devices into a single fiber. In contrast, the composite preform-to-fiber approach pioneered in our group addresses the key challenges of device density and fiber length simultaneously. It allows one to construct structured fibers composed of metals, insulators and semiconductors and enables the incorporation of many devices into a single fiber capable of performing complex tasks such as of angle of incidence and color detection. However, until now, devices built by the preform-to-fiber approach have demonstrated only ohmic behavior due to the chalcogenide semiconductor's amorphous nature and defect density. From a processing standpoint, non-crystallinity is necessary to ensure that the preform viscosity during thermal drawing is large enough to extend the time-scale of breakup driven by surface tension effects in the fluids to times much longer than that of the actual drawing. The structured preform cross-section is maintained into the microscopic fiber only when this requirement is met. Unfortunately, the same disorder that is integral to the fabrication process is detrimental to the semiconductors' electronic properties, imparting large resistivities and effectively pinning the Fermi level near mid-gap. Indeed, the defect density within the mobility gap of many chalcogenides has been found to be  $10^{18}$ - $10^{19}$  cm<sup>-3</sup> eV<sup>-1</sup>, resulting in a narrow depletion width and ohmic behavior at metals-semiconductor junctions. In this work we incorporated phase-changing semiconductors, those that may be easily converted between the amorphous and crystalline states, into composite fibers with a goal towards constructing *rectifying junctions* in fiber.

Indeed, with proper selection of the semiconductor and the metallic contacts, we demonstrate here the first arbitrarily long rectifying junction in the form of a distributed photodiode.

The fiber device was constructed in the standard method of multimaterial device fabrication. A macroscopic preform, consisting of metal electrodes, a semiconductor film and insulating polymer, is built and thermally drawn down into tens of meters of fiber (see methods for further detail). Figure 1 depicts schematic drawings of the preform and resulting device fiber along with scanning electron microscope (SEM) micrographs of the final fiber and a magnification of an individual metal-semiconductor-metal device. The distance between the electrodes in a single device is approximately 15  $\mu\text{m}$ , an order of-magnitude smaller than previous multimaterial device fibers. The semiconductor film that spans the distance between the electrodes is crystalline selenium modified with 3 at% sulfur to depress the alloy melting temperature. The selenium-sulfur alloy is an unstable glass. Upon exiting the drawing furnace the semiconductor is quenched into the amorphous state, but it easily devitrifies to the equilibrium *crystalline state* by an *additional annealing step for one hour at 150 °C*. The semicircular electrodes are composed of two eutectic alloys, Sn<sub>74</sub>Pb<sub>26</sub> and Sn<sub>85</sub>Zn<sub>15</sub> at% (Sn<sub>63</sub>Pb<sub>37</sub> and Sn<sub>91</sub>Zn<sub>9</sub> wt%, respectively) placed in an alternating fashion, so that each Sn<sub>74</sub>Pb<sub>26</sub> – Se<sub>97</sub>S<sub>3</sub> – Sn<sub>85</sub>Zn<sub>15</sub> combination forms an independent device. The metal alloy components have very small solubility in each other at room temperature and are essentially segregated into elemental phases (large lead-rich phases are easily seen as bright spots in the SEM micrographs, zinc phases are small and evenly dispersed, making them less visible).

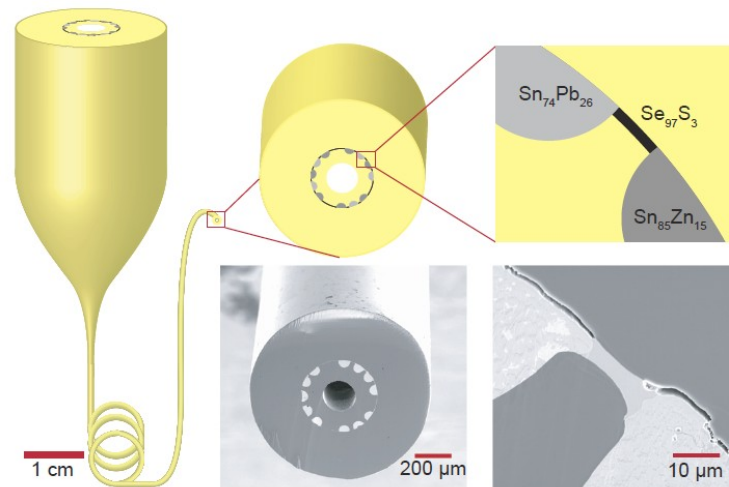


*Figure 1. Schematic drawings of structured preform drawn into fiber along with SEM micrographs of actual fiber and magnification of a single metal-semiconductor-metal junction.*

The fiber diode optoelectronic properties are characterized in figure 2. The current-voltage characteristics per unit fiber length as a function of voltage both in the dark and under illumination from a simulated AM1.5G solar source is given in figure 2a. The Sn<sub>74</sub>Pb<sub>26</sub> electrode is biased positive with respect to the Sn<sub>85</sub>Zn<sub>15</sub> electrode in the forward direction (inset fig. 2a). Rectifying behavior is clearly evident in the dark, the

magnitude of which is limited by the device series resistance arising from the lateral photodiode geometry. A short-circuit current and open-circuit voltage (0.5V) develops under illumination, demonstrating the existence of an internal electric field and suggesting future application as a distributed photovoltaic device. The active region of the diode in this lateral geometry is limited to the depletion region plus one diffusion length from the region rather than the entire distance between the electrodes. As the both the depletion and diffusion lengths in typical polycrystalline selenium device are on the order of one micron or less the power conversion efficiency is estimated to be around 0.01%. A plot of the inverse square capacitance versus applied bias reveals a built-in voltage of about 0.8 V (figure 2b). A dispersion in the C-V measurements at different frequencies was observed (not shown), indicative of a large density of interfacial states. The spectral responsivity shown in figure 2c under reverse bias (-2V) shows maximum response in the green (corresponding to an external quantum efficiency of about 2%) and a trail off at around 650nm, consistent with a selenium bandgap of about 1.9 eV. The decreased responsivity at short wavelengths is due to a combination of shorter penetration depth of the high energy photons and traps and recombination centers at the polymer/semiconductor interface.

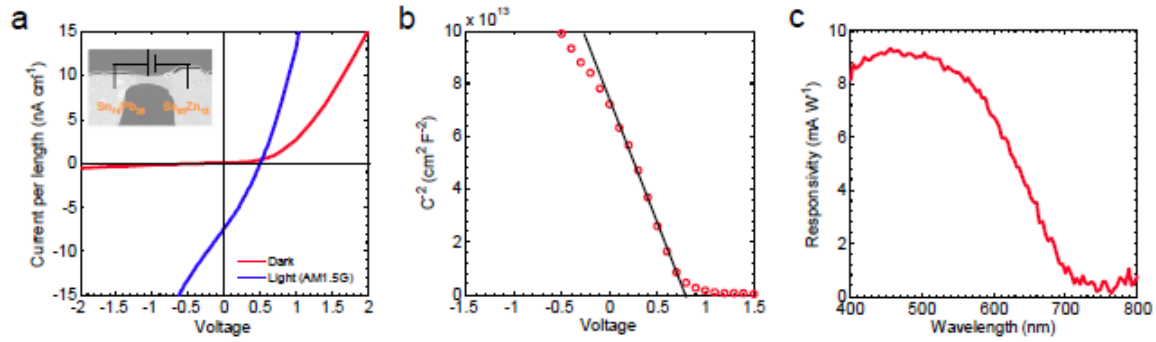


*Figure 2. Characterization of fiber integrated photodiode. (a) Current per length for distributed photodiode in the dark and under illumination from simulated AM1.5G source (inset shows bias polarity). (b) Inverse square of capacitance as a function of applied voltage reveals a junction built-in voltage of 0.8 V. (c) Responsivity as a function of wavelength.*

The fact that the I-V and C-V characteristics suggest a one-sided device, i.e. a device composed of one ohmic and one blocking barrier, may seem counterintuitive because of the large work function difference between the semiconductor and metals. Polycrystalline selenium is known to be a p-type semiconductor having a work function typically around 5.9 eV. While other elemental semiconductors such as silicon and germanium have surface states that lead to a weak relationship between metal semiconductor work function difference and barrier height, selenium shows a rather large dependence. The work function of the Sn<sub>85</sub>Zn<sub>15</sub> electrode has been shown to be 3.9 and 4.2 eV by ultraviolet photoemission spectroscopy (UPS) and the Kelvin Probe technique,

respectively. Using the same methods, the Sn74Pb26 work function is approximately 4.2 and 4.5 eV, respectively. Given the almost 2 eV difference in work functions between metal and semiconductor, it seems especially surprising that the metal-semiconductor junction behave differently. Because selenium is a p-type semiconductor, the polarity of the I-V and C-V measurements imply that the Sn74Pb26 / Se97S3 junction behaves ohmically while the Se97S3 / Sn85Zn15 interface forms the blocking barrier. Furthermore, similar devices were fabricated with several other metal electrodes, but only fibers containing Sn85Zn15 showed rectification. Greater understanding into the origin of the electronic behavior of these junctions in their fiber form may be gained by direct examination of the composition and potential variation across the metal-semiconductor interfaces.

The spatial variation in surface potential may be directly measured by Kelvin probe force microscopy (KPFM) and compared with compositional measurements performed by energy dispersive spectroscopy (EDS). KPFM is a non-contact atomic force microscope technique that enables the simultaneous measurement of both topography and surface potential. Our KPFM map and line scans show the potential change occurs over a 400 nm region at the interface. Our EDS measurements reveal notable diffusion of tin and selenium at the interface as well as a small increase in concentration of lead at the interface. On the other hand, the band bending extends over 1  $\mu\text{m}$  at the Se97S3 / Sn85Zn15 interface, beginning with an abrupt change in contact potential at the 2.5  $\mu\text{m}$  mark and followed by a more gradual change. The topography map, however, reveals the metallurgical Se97S3 / Sn85Zn15 junction occurs roughly at the 1.1  $\mu\text{m}$  mark. EDS line scans show a large increase in zinc concentration at the metallurgical interface.

The combination of the EDS and KPFM data suggest that electronic behavior of the interfaces is guided by mixing and/or compound formation of the metal and semiconductor. The Sn74Pb26 / Se97S3 junction behaves ohmically despite the large potential drop observed by KPFM. EDS demonstrates that this interface is not sharp, and the presence of lead may also be a contributing factor. By itself, lead would be expected to act as a p-type donor in selenium, increasing the carrier density at the interface, possibly enough to create an ohmic tunnel junction. But the diffuse interface is a classic method of creating ohmic contacts between metals and semiconductors. The Se97S3 / Sn85Zn15 interface is more interesting. Even though the region in panel b between 1.1 and 2.5  $\mu\text{m}$  appears as though it has the same topography as the metal, it must be composed of semiconductor because the band bending clearly visible in the KPFM map cannot occur in high carrier density metals. The EDS measurements reveal the large change in zinc composition at the metallurgical interface, suggesting that this compound may be zinc-selenide-based. Another possible compound, SnSe2 can be ruled out because there were no signs of compound formation at the Sn74Pb26 / Se97S3 even though SnSe2 would be just as likely to form at either interface. A large bandgap semiconductor such as zinc selenide ( $E_g = 2.7$  eV, I.P. = 6.8 eV) would form a barrier to hole conduction and explain the rectifying behavior, as can be seen from a preliminary band diagram of the Se97S3 / ZnSe / Sn85Zn15 heterostructure in figure 3. The diagram is constructed by combining knowledge of the semiconductors' bandgap and ionization potential (I.P.  $\sim 6.0$  to 6.1 eV for selenium), electron affinities and the observed change in contact potential

across the junction. The discontinuity in the valence and conduction bands is determined by Anderson's model of heterostructures. A large density of interface states is expected at both interfaces (represented by dashed lines) due to differences in lattice constant ( $a_{\text{Sn}} = 5.83 \text{ \AA}$ ,  $c_{\text{Sn}} = 3.19 \text{ \AA}$ ,  $a_{\text{Se}} = 4.36 \text{ \AA}$ ,  $c_{\text{Se}} = 4.95 \text{ \AA}$ ,  $a_{\text{ZnSe}} = 5.67 \text{ \AA}$ ) between the materials and the observed dispersion in capacitance measurements at different frequencies. The proposed band diagram clearly indicates how the large discontinuity in the valence band at the  $\text{Se}_{97}\text{S}_3$  /  $\text{ZnSe}$  interface would create a barrier to hole flow.

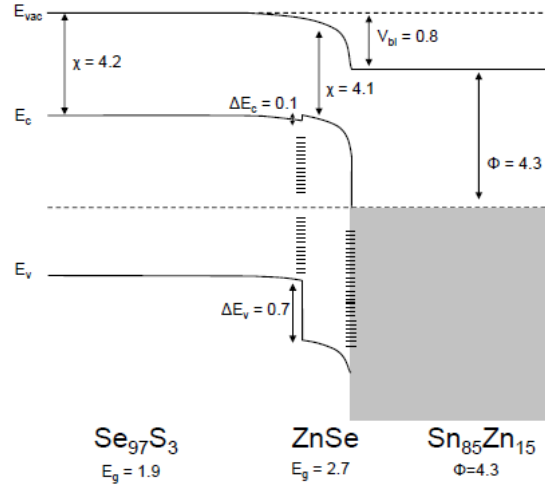


Figure 3. Proposed Band diagram of the  $\text{Se}_{97}\text{S}_3$  /  $\text{ZnSe}$  /  $\text{Sn}_{85}\text{Zn}_{15}$  heterostructure (values in eV).

This method of compound formation in the fiber is not unlike the formation of silicides at silicon and metal interfaces that have revolutionized microelectronics and suggests that many more materials can be built into these composite fibers than previously thought. Zinc selenide has many interesting optical and electronic properties but melts at  $1530^\circ\text{C}$  and thus would never have been considered as a suitable material for thermal drawing at low temperatures. It is likely that other technologically relevant compound semiconductors such as  $\text{CdSe}$ ,  $\text{InSe}$  or even  $\text{InAs}$  may be incorporated into fibers with a similar method. One must only identify compounds that may be fluid processed together that could be converted to others.

The ability to design electronic contacts within extended lengths of optical fiber devices is a milestone in fiber device processing. Introduction of new materials into multimaterial fiber processing has the potential to be even more important because it offers a greater degree in freedom in constructing advanced fiber devices. By proper selection of the semiconductor and metal electrodes both ohmic and rectifying junctions can be fabricated, and a distributed photodiode was demonstrated by creating a selenium / zinc selenide heterostructure. Simple devices such as this are important building blocks of electronic circuits, and this work should enable significant advances in the function fiber devices on both the individual and array level.

***Publications during this final period:***

1. Orf, ND, Baikie, ID, Shapira, O, Fink, Y, "Work Function Engineering in Low-Temperature Metals," *Applied Physics Letters* **94** 113504 (2009).
2. F. Sorin, O. Shapira, A. F. Abouraddy, Matthew Spencer, Nicholas D. Orf, J. D. Joannopoulos, Y. Fink, "Exploiting Collective effects of multiple Optoelectronic Devices Integrated in a Single Fiber" *F. Nano Lett.*, **9** , 2630 (2009).